

Herschel-SPIRE: Design, Performance, and Scientific Capabilities

Matthew Griffin^{*,a}, Alain Abergel^b, Peter Ade^a, Philippe André^c, Jean-Paul Baluteau^d, James Bock^e, Alberto Franceschini^f, Walter Gear^a, Jason Glenn^g, Douglas Griffin^h, Ken King^h, Emmanuel Lellouchⁱ, David Naylor^j, Göran Olofsson^k, Ismael Perez-Fournon^l, Michael Rowan-Robinson^m, Paolo Saracenoⁿ, Eric Sawyerⁱ, Alan Smith^o, Bruce Swinyardⁱ, Laurent Vigroux^p, and Gillian Wright^q

^aSchool of Physics and Astronomy, Cardiff University, 5 The Parade, Cardiff CF24 3YB, UK;

^bInstitut d'Astrophysique Spatiale, Orsay, France;

^cService d'Astrophysique, CEA, Saclay, France ;

^dObservatoire de Marseille, France ;

^eJet Propulsion Laboratory, Pasadena, California, USA;

^fUniversità di Padova, Italy;

^gUniversity of Colorado, Boulder, Colorado, USA;

^hRutherford Appleton Laboratory, Oxfordshire, UK;

ⁱObservatoire de Paris, France;

^jUniversity of Lethbridge, Lethbridge, Alberta, Canada;

^kStockholm Observatory, Sweden;

^lInstituto de Astrofísica de Canarias, Tenerife, Spain;

^mImperial College, University of London, UK;

ⁿIstituto di Fisica dello Spazio Interplanetario, Rome, Italy;

^oMullard Space Science Laboratory, Surrey, UK;

^pInstitut d'Astrophysique de Paris, France;

^qUK Astronomy Technology Centre, Edinburgh, UK.

ABSTRACT

SPIRE, the Spectral and Photometric Imaging Receiver, is a submillimetre camera and spectrometer for the European Space Agency's Herschel Space Observatory. It comprises a three-band imaging photometer operating at 250, 360 and 520 μm , and an imaging Fourier Transform Spectrometer (FTS) covering 200-670 μm . The detectors are arrays of feedhorn-coupled NTD spider-web bolometers cooled to 0.3 K. The photometer field of view is 4 x 8 arcmin., observed simultaneously in the three spectral bands. The FTS has an approximately circular field of view with a diameter of 2.6 arcmin., and employs a dual-beam configuration with broad-band intensity beam dividers to provide high efficiency and separated output and input ports. The spectral resolution can be adjusted between 0.04 and 2 cm^{-1} (resolving power of 20-1000 at 250 μm). The flight instrument is currently undergoing integration and test. The design of SPIRE is described, and the expected scientific performance is summarised, based on modelling and flight instrument test results.

Keywords: Herschel, Far Infrared, Submillimetre, Instrumentation

* E-mail: matt.griffin@astro.cf.ac.uk; Telephone: +44-(0)29-2087-4203; Fax: +44-(0)29-2087-4056

1. INTRODUCTION

The European Space Agency's Herschel Space Observatory¹ is scheduled for launch in 2008. Its main scientific goals are the statistics and physics of galaxy and structure formation at high redshift and the study of the early stages of star formation. These scientific investigations require deep imaging surveys at far-infrared (FIR) and submillimetre wavelengths, and photometry and spectroscopy of individual sources.

Galaxies emit much of their energy in the FIR due to the heating of interstellar dust grains by accretion energy and stellar UV radiation. The FIR emission is redshifted into the submillimetre for galaxies with redshift, z , greater than ~ 1 . Determining a galaxy's total luminosity requires measurement of its Spectral Energy Distribution (SED), and the study of the early stages of galaxy evolution thus needs detection of high- z galaxies in the submillimetre, enabling their SEDs and luminosities to be derived. In our own galaxy, star formation occurs through fragmentation and collapse of dense cloud cores in the interstellar medium (ISM), and the early stages of this process are poorly understood and difficult to observe directly. FIR and submillimetre observations with high spatial resolution are needed to make sensitive surveys of protostellar clumps to determine their bolometric luminosities and mass function. Herschel's high sensitivity to cold dust and the stable observing conditions of a space observatory also make it ideal for studying faint extended emission from material that has been ejected from evolved stars, enriching the interstellar medium with heavy elements.

SPIRE is designed to exploit the particular advantages of Herschel: its large-aperture (3.5 m), cold, (~ 80 K), low-emissivity (a few %) telescope; unrestricted access to the poorly explored 200-700- μm range; and the large amount of high quality observing time. Although the instrument design is dictated by these two main science themes, it will offer a powerful tool for many other astrophysical studies: giant planets, comets, the galactic interstellar medium, nearby galaxies, ultraluminous infrared galaxies, and active galactic nuclei. Its capabilities will remain unchallenged by the ground-based and the airborne observatories which are planned to come into operation over the next decade.

2. INSTRUMENT OVERVIEW

SPIRE contains a three-band imaging photometer and an imaging Fourier Transform Spectrometer (FTS), both of which use bolometer arrays operating at 0.3 K. The photometer field of view is 4×8 arcmin., the largest that could be achieved given the location of the SPIRE field of view in the Herschel focal plane and the size of the telescope unvignetted field of view. Three bolometer arrays are used for broad-band photometry ($\lambda/\Delta\lambda \sim 3$) in spectral bands centred on approximately 250, 360 and 520 μm . The same field of view is observed simultaneously in the three bands through the use of two fixed dichroic beam-splitters. Signal modulation can be provided either by SPIRE's two-axis Beam Steering Mirror (BSM) or by scanning the telescope across the sky. An internal thermal source is available to provide a repeatable calibration signal for the detectors. The FTS has spatially separated input and output ports. One input views a 2.6-arcminute diameter field of view on the sky and the other is fed by an on-board reference source. Two bolometer arrays at the output ports cover 200-325 μm and 315-670 μm . The FTS spectral resolution is set by the total optical path difference, and can be adjustable between 0.04 and 2 cm^{-1} (corresponding to $\lambda/\Delta\lambda = 1000 - 20$ at 250 μm).

The photometer and spectrometer both have cold pupil stops conjugate with the Herschel secondary mirror, which is the system pupil for the telescope and defines a 3.29-m diameter used portion of the primary. Feedhorns provide a roughly Gaussian illumination of the pupil, with an edge taper of around 8 dB in the case of the photometer arrays.

The SPIRE focal plane unit (FPU) is approximately 700 x 400 x 400 mm in size and is supported from the 10-K cryostat optical bench by thermally insulating mounts. The FPU has three temperature stages: the Herschel cryostat provides temperatures of 4.5 K and 1.7 K via high thermal conductance straps to the instrument, and an internal ³He refrigerator cools all five detector arrays to approximately 0.3 K. Two sets of JFET preamplifiers are used to read out the bolometer signals, one for the photometer and one for the spectrometer. The JFET units are attached to the 10-K optical bench next to the 4.5-K enclosure, with the JFETs heated internally to their optimum operating temperature of ~ 120 K.

There are three SPIRE warm electronics units: the Detector Control Unit (DCU) provides the bias and signal conditioning for the arrays and cold electronics, and demodulates and digitises the detector signals; the FPU Control Unit (FCU) controls the ³He cooler and the two FPU mechanisms, and reads out all the FPU thermometers; and the Digital Processing Unit (DPU) runs the on-board software interfaces with the spacecraft for commanding and telemetry.

The 130 kbs available data rate allows all photometer or spectrometer detectors to be sampled and the data transmitted to the ground with no on-board processing.

3. THREE-BAND IMAGING PHOTOMETER

3.1 Optical design and layout of the photometer

Optics: Figure 1 shows the layout of the photometer. The 4.5-K optics are mounted on the SPIRE internal optical bench. (The input optics are common to the photometer and spectrometer and the separate spectrometer field of view is directed to the other side of the optical bench panel by a pick-off mirror.) The 1.7-K enclosure contains the detector arrays, dichroics and fold mirrors. The bolometer array modules of the photometer are bolted to the outside wall of the 1.7-K box. Inside each one, the ^3He stage, accommodating the detectors, feedhorns and final filters, is thermally isolated from by tensioned Kevlar threads, and cooled by a thermal strap to the ^3He cooler.

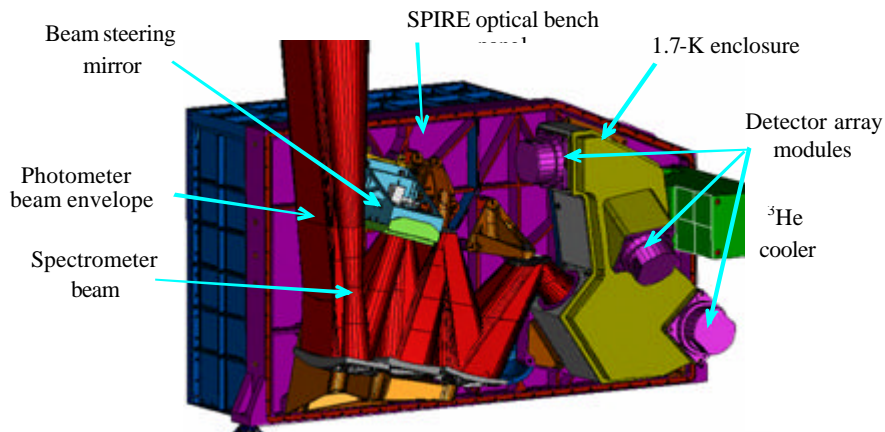


Figure 1: Computer-generated image of the SPIRE photometer layout.

The photometer optical design² is shown in Fig. 2. It is all-reflective except for the dichroics used to direct the three bands onto the bolometer arrays, and the filters used to define the passbands. The image is diffraction-limited over the 4×8 arcmin. field of view, which is offset by 11 arcmin. from the centre of the Herschel telescope's highly curved focal surface. Input mirror M3 lying below the telescope focus, receives the $f/8.7$ telescope beam and forms an image of the secondary at the flat beam steering mirror, M4. Mirror M5 converts the focal ratio to $f/5$ and provides an intermediate focus at M6, which re-images the M4 pupil to a cold stop. Mirrors M7, M8 and M9 form a one-to-one optical relay to bring the M6 focal plane to the detectors. M3 - M8 are at 4.5 K and the cold stop and all subsequent optics are at 1.7 K.

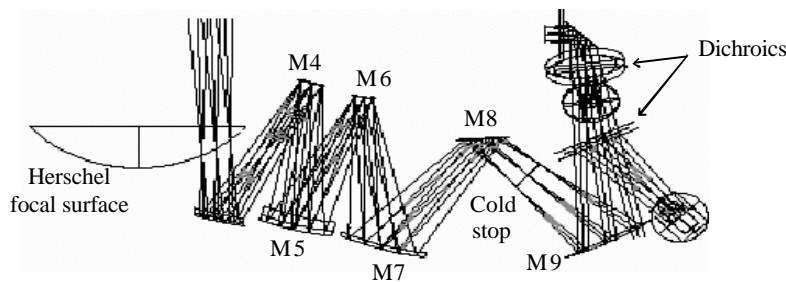


Figure 2: SPIRE photometer optical design.

Internal calibration source: An internal thermal source^{3,4} is used to provide a repeatable signal for the bolometers. It is not designed to provide an absolute calibration - that will be done by observing standard astronomical sources. It radiates through a 2.8-mm hole in the centre of M4, occupying an area contained within the region of the pupil obscured by the hole in the primary. The source can produce a power at the detector of 1-2% of the telescope background. The latter is typically a few pW, so the signal level is a few $\times 10^{-14}$ W. With a detector NEP of a few $\times 10^{-17}$ W Hz^{-1/2}, this gives a large instantaneous S/N. Mirror M4 is at a pupil, so the illumination is close to uniform over the arrays.

Beam steering mirror: M4, the beam steering mirror⁵ can chop ± 2 arcmin. along the long axis of the 4 x 8 arcmin. field of view, at frequencies up to 5 Hz. It can simultaneously chop at up to 1 Hz in the orthogonal direction by up to 30". This two-axis motion allows "jiggling" of the pointing to create a fully sampled image of the sky with the feedhorn coupled detectors whose diffraction-limited beams on the sky are separated by approximately twice the beam FWHM.

Filters and dichroics: Quasi-optical filters⁶ define the bands with high out-of-band rejection, and minimise the thermal load on the low-temperature stages by reflecting short-wavelength radiation. For high rejection out to UV wavelengths, four blocking filters are needed in the chain. The bands are defined by a combination of transmission edges (of filters in front of the detectors), reflection/transmission edges of the dichroics, and the cutoff wavelengths of the feedhorn output waveguides. The three bands are centred at 250, 363 and 517 μ m, with $I/\Delta I$ of 3.0, 3.2, and 3.0, respectively.

Bolometer arrays: The SPIRE detectors⁷⁻¹⁰ are spider-web bolometers using NTD germanium thermometers, which are coupled to the telescope by hexagonally close-packed $2FI$ -diameter single-mode conical feedhorns, giving diffraction limited beams of FWHM 18, 25 and 36" for the 250, 360 and 520- μ m bands respectively.

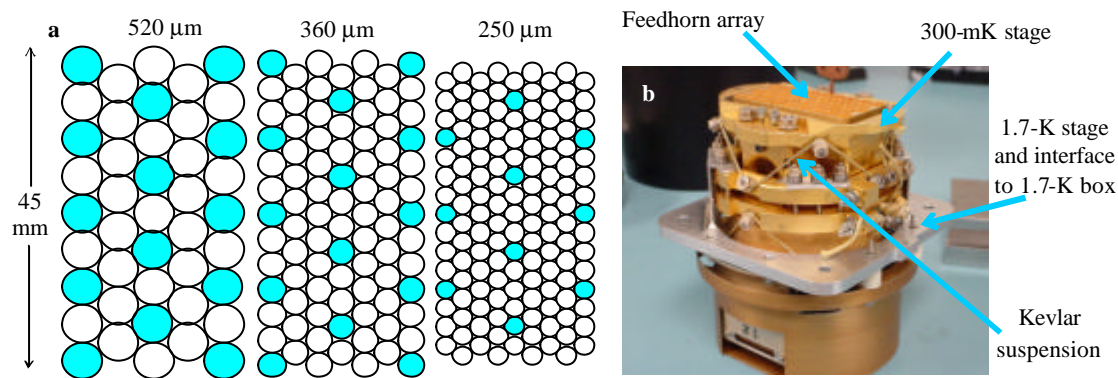


Figure 3: (a) Layout of the photometer arrays. The shaded detectors are those for which there is exact overlap on the sky for the three bands; (b) SPIRE PLW detector array module

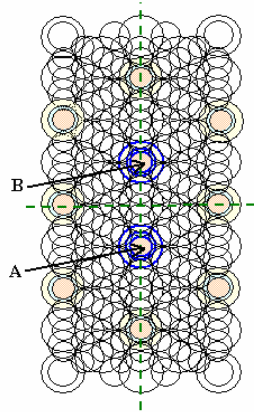
The three arrays (see Fig. 3) contain 43 (520 μ m), 88 (360 μ m) and 139 (250 μ m) detectors. The array layouts are shown schematically in Fig. 4a, and Fig. 4b is a photograph of an array module. Each unit has an identical interface to the 1.7-K box and a thermal strap from the ³He cooler to the 0.3-K stage, which is supported by Kevlar cords from the 1.7-K level. Connections to the detectors are made with Kapton ribbon cables inside the array modules and with woven manganin cables between the arrays and the JFETs. The bolometers are AC-biased with frequency adjustable over the range 50 - 300 Hz, reducing $1/f$ noise from the JFET readout, and giving a $1/f$ knee for the system of less than 100 mHz.

3.2 Observing modes for the imaging photometer

The photometer will have three principal observing modes¹¹, as illustrated in Fig. 4 and described below.

Point or compact source photometry: Several sets of three detectors have beams at the three wavelengths that are co-aligned on the sky (shaded circles in Fig. 3). By chopping through an angle of 126", three-band photometry can be carried out with maximum efficiency: the source is observed in one of the detectors in each band at all times. The

absolute pointing uncertainty of Herschel is 3.7" (requirement) and 1.5" (goal). If the goal is achieved, then the rms signal loss in the case of SPIRE's narrowest beam (18") is 2% at worst. But if the error is at the level of the requirement,



Point source observation:

- $\pm 63''$ chop between A and B
- Standard 7-point jiggle

Field map (4 x 4 arcmin):

- $\pm 120''$ chop
- 64-point jiggle

Scan map:

- 4 x 8 arcmin. Field of view
- No chop or jiggle
- Telescope scanned at 12.5° with respect to the array axes

Figure 4: Photometer observing modes

then the loss of signal can be more than 10% - unacceptable for many applications. It may also be necessary to ensure that imperfect knowledge of the source position does not affect the photometric accuracy. For these reasons, the standard observing mode for point sources will use the beam steering mirror to make a seven-point map in which the nominal position and six hexagonally arranged neighbouring positions are observed in turn. With an angular offset of 6", the S/N loss for a given integration time is about 20% in the worst case (250 μm band). This is a small price to pay for assurance that pointing or source position errors do not result in flux density errors. The data from all detectors in all of the arrays will also be transmitted to the ground, providing sparsely sampled maps of the field around the object.

Field mapping: For mapping of regions a few arcmin. in size, the beam steering mirror will perform a jiggle map, similar to the mode of operation of the SCUBA bolometer camera on the JCMT¹². A 64-point jiggle pattern is needed to achieve full spatial sampling in all bands simultaneously, with a step size of 9" (half-beam spacing at 250 μm). The 250- μm band image will be critically sampled, and the other two will be oversampled. A maximum field size of 4 x 4 arcmin. is available in this mode as the 2-arcmin. regions at each end of the array will be chopped outside the field of view admitted by the photometer optics.

Scan mapping: This mode will be used for large maps (bigger than the SPIRE field of view), including deep surveys. The telescope will be scanned across the sky at up to 1 arcmin. s^{-1} (the maximum rate that the spacecraft can provide). The nominal scan rate is currently taken to be 30" s^{-1} . The good $1/f$ stability of the detectors means that the beam steering mirror does not need to be operated - signal modulation is provided by the telescope motion. To give the beam overlap needed for full spatial sampling over a strip defined by one scan line, and to provide a uniform distribution of integration time over the area covered by the scan, the optimum scan angle is 12.5° with respect to one of the array axes.

4. IMAGING FOURIER TRANSFORM SPECTROMETER

4.1 Optical design and layout of the spectrometer

The FTS¹³⁻¹⁷ uses two broadband intensity beam splitters in a Mach-Zehnder configuration. All four ports of the interferometer are independently accessible as in the Martin-Puplett (M-P) polarising FTS. But the throughput is a factor of two higher than for the M-P as none of the incoming radiation is rejected, and there is no sensitivity to the polarisation of the incident radiation. A thermal source at the second input port allows the background power from the telescope to be matched. The amplitude of the interferogram central maximum is proportional to the difference in the radiant power from the two ports, so this allows the large telescope background to be nulled, reducing the dynamic range requirements for the detector sampling. Detector arrays are placed in the two output ports, with overlapping bands of 200-325 μm and

315-670 μm . A single back-to-back scanning roof-top mirror serves both interferometer arms. It has a frictionless mechanism using double parallelogram linkage and flex pivots, and a Moiré fringe sensing system

FTS optics: The focal plane layout of the FTS is shown in Fig. 5 and the optical design is illustrated in Fig. 6. The spectrometer beam enters through a hole in the panel into the FTS side of the instrument. A pupil stop is located between the pick-off mirror and the input fold mirror. The input relay mirror brings the beam to an intermediate focus just after the first beam divider, after which the beam is collimated and sent to the moving roof-top mirror. The roof-top shifts the beam and sends it towards the camera mirror, which produces an image just before the output beam divider. A pupil is located near the final fold mirror, making this a convenient location for the entrance to the 1.7-K enclosure. This pupil moves when the optical path difference changes, so it is not suitable for a limiting cold stop. Instead, the limiting aperture is located at the 4.5-K pupil between the pick-off mirror and the input fold mirror. The output relay mirror focuses the beam onto the detector arrays. Each array has a lens incorporated in its 0.3-K filter stack to correct for the non-telecentric FTS optics and provide more uniform fringe contrast and efficiency across the field.

Filters: A filtering scheme similar to the one employed for the photometer channel is used to restrict the passband of the instrument. The bands cover 200-325 μm (SSW) and 315-670 μm (SLW), overlapping at the 90% level.

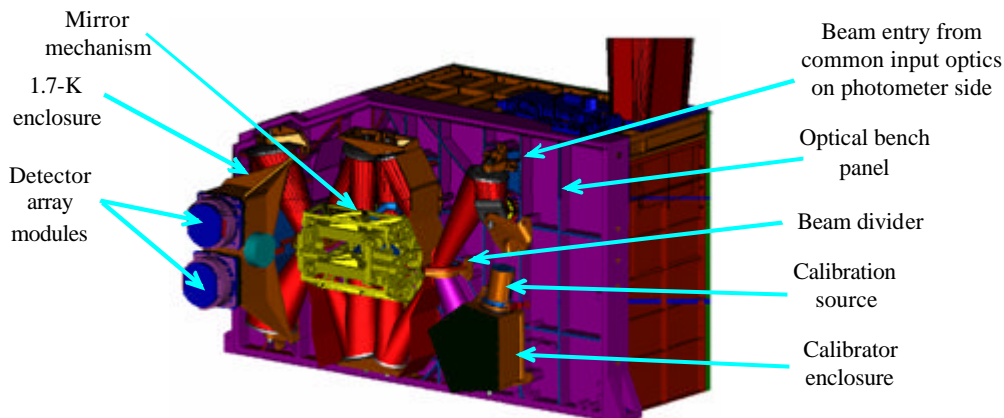


Figure 5: Computer-generated image of the SPIRE FTS layout

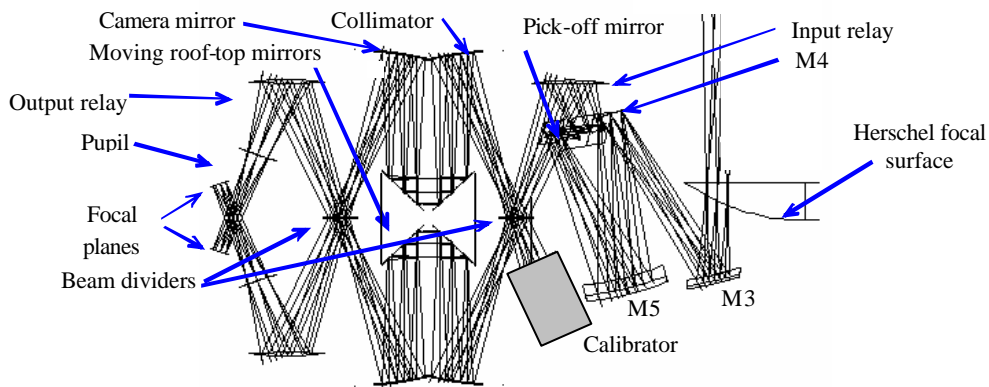


Figure 6: Optical design of the FTS.

FTS detector arrays: The two spectrometer arrays contain 37 hexagonally close-packed detectors in the short-wavelength array and 19 in the long-wavelength array. The array modules are similar to those used for the photometer, with an identical interface to the 1.7-K enclosure. The layout of the FTS arrays is shown schematically in Fig. 7. The detectors on the periphery are partly vignettted by the 2.6-arcminute field of view admitted by the instrument optics (shown by the large circles in Fig. 7). The feedhorn and detector cavity designs are carefully optimised to provide good sensitivity across the whole wavelength range of the FTS. The SSW feedhorns are sized to give $2FI$ pixels at $225\ \mu\text{m}$ and the SLW horns are $2FI$ at $389\ \mu\text{m}$. This arrangement has the advantage that there are many co-aligned pixels in the combined field of view. The SSW beams on the sky are $27''$ apart, and the SLW beams are separated by $48''$. Detailed analysis of the beam profiles an their wavelength dependence is complex due to the multimoded nature of the horns, and has yet to be carried out. Preliminary calculations indicate that the FWHM will vary between $20 - 25''$ across the short-wavelength band and $30 - 50''$ across the longer wavelength band.

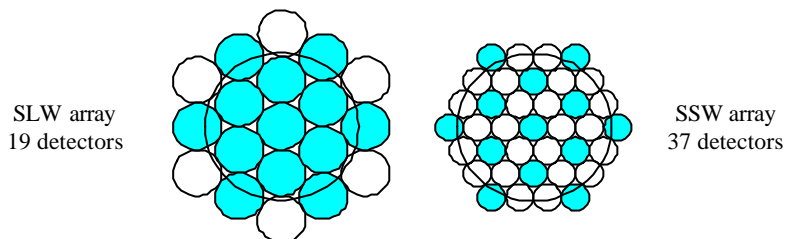


Figure 7: Spectrometer detector arrays. The shaded detectors are co-aligned on the sky in the two bands.

4.2 FTS operating modes

The spectral resolution can be adjusted between 0.04 and $2\ \text{cm}^{-1}$ ($I/\Delta I = 1000-20$ at $250\ \mu\text{m}$), by setting the scan length. For point sources, the object will be positioned at the centre of the array, but data will be acquired for all of the detectors, providing at the same time a sparsely-sampled map of the emission from the region around the source. Likewise, a single pointing will give a sparsely-sampled map of an extended object. For fully-sampled spectral mapping, the beam steering mirror will provide the necessary pointing changes between scans. The FTS can be operated in two modes:

Continuous scan: In this case the beam steering mechanism is stationary and the scan mirror is moved (nominally at $0.5\ \text{mm s}^{-1}$, giving an optical path rate of $2\ \text{mm s}^{-1}$ due to the factor of four folding in the optics). Radiation frequencies of interest are encoded as detector output electrical frequencies in the range $3-10\ \text{Hz}$. The maximum scan length is $3.5\ \text{cm}$, corresponding to an optical path difference of $14\ \text{cm}$. To ensure that mechanism jitter noise is well below the photon noise level, the mirror position has a relative accuracy of $0.1\ \mu\text{m}$. The need to null the strong telescope background means that the FTS calibration source has to be on continuously.

Step-and-integrate: In this mode, the scan mirror is placed in turn at a set of positions to form a scan. Steps of less than $5\ \mu\text{m}$ physical travel are needed for good over-sampling of the interferogram. Scans are repeated until the desired total integration time is reached. The reference source can be off because the telescope background is chopped out by the beam steering mechanism. In principle, this mode gives higher S/N by a factor of $\sqrt{2}$ as the calibrator does not need to be operating, reducing photon noise. However, continuous scan is usually the chosen mode for an FTS as it minimises the effects of $1/f$ noise and reduces the time overhead due to moving the mirror between positions. In addition, the source is referenced against the known internal calibrator rather than an adjacent region of sky. Which mode is better in practice will depend on the overall system performance and noise characteristics and the type of observation. Step-and-integrate may be optimal for low resolution spectrophotometry and continuous scan for higher resolution line spectroscopy.

5. ^3He COOLER AND 300-MK THERMAL STRAP SYSTEM

The same ^3He cooler design¹⁸ will be used for both the SPIRE and PACS instruments. Gas gap heat switches control the cooler and there are no moving parts. Liquid confinement in zero-g is achieved by a porous material which holds the liquid by capillary attraction. A Kevlar wire suspension supports the cooler during launch whilst minimising the

parasitic heat load. The cooler contains 6 STP litres of ^3He , fits in a 200 x 100 x 100-mm envelope and weighs about 1.7 kg. Operating from 1.7 K, it achieves a temperature of 274 mK with a 10- μW load and a 46 hr hold time, and a total time-averaged power load on the 1.7 K heat sink of ~ 3 mW. Copper straps connect the 0.3-K stage to the five detector arrays, and are held rigidly at various points by Kevlar support modules¹⁹. The supports at the entries to the 1.7-K boxes are also designed to be light-tight. The cooler will be recycled during periods when the Herschel telemetry antenna is pointed towards Earth for data downlink and command uplink. In these ~ 3 -hr periods, operation of the instruments is not planned due to possible interference from the transponder operation and the highly restricted pointing.

6. INSTRUMENT PERFORMANCE ESTIMATES

The sensitivity of SPIRE has been estimated under the assumptions listed below in Table 1. Various other parameters are taken into account including telescope motion overheads, chopping efficiency, and JFET and warm amplifier noise. The nominal background power levels on the detectors (which are dominated by the telescope), and the corresponding photon noise limited NEP values are given in Table 2 and the instrument sensitivities are summarised in Table 3

Telescope	Temperature (K)	80			Notes
	Effective emissivity	0.04			a
	Used diameter (m)	3.29			
	Obscuration factor	0.87			b
Photometer	Band centre wavelengths (μm)	250	363	517	
	Filter widths ($\lambda/\Delta\lambda$)	3.0	3.2	3.0	
	Bolometer Detective Quantum Efficiency	0.66	0.57	0.47	c
	Overall feed efficiency (fundamental mode)	0.70	0.70	0.70	d
	Throughput	λ^2			e
	Aperture efficiency	0.7			f
	Spillover efficiency	0.8			g
	Bolometer operating temperature (K)	0.32			h
	Array yield	0.8			i
	Overall instrument transmission	0.4			j
	FTS	Bands (μm)	200 – 325	315 – 670	
Bolometer Detective Quantum Efficiency		0.70	0.65		c
Overall feed efficiency (fundamental mode)		0.70	0.70		d
Aperture efficiency		0.70	0.70 – 0.5		f
Spillover efficiency		0.80	0.80 – 0.6		g
Throughput (for signal)		λ^2			e
Bolometer operating temperature (K)		0.32			h
Maximum spectral resolution (cm^{-1})		0.04			
Overall instrument transmission		0.15			j
Signal modulation efficiency		0.50			
Electrical filter efficiency		0.80			

Table 1: Assumptions for sensitivity estimation.

Notes to Table 1:

- a The telescope reflectors are expected to have an emissivity $< 1\%$ each. The assumed overall emissivity of 4% allows pessimistically for substantial additional background radiation due to stray light.
- b The effective collecting area of the telescope is reduced due to the hole in the primary and the shadows cast by the secondary support structure. The loss of throughput is accounted for by a single obscuration factor, calculated by

- convolving the obscuration pattern with an 8-dB Gaussian taper.
- c The bolometer DQE estimates are based on modelling and on the performance levels achieved by bolometer arrays manufactured to date.
 - d The overall feed efficiency takes into account the losses in the feedhorn and in the coupling of the radiation to the bolometer inside its integrating cavity. The background power on the detectors is calculated taking all propagated modes into account, but signal power is assumed (pessimistically) to be confined to the fundamental mode.
 - e The throughput is taken to be I^2 , corresponding to single-mode operation, for the photometer detectors. For the FTS, the feedhorns admit various additional modes for parts of the bands. The background power on the detectors is calculated taking these additional modes into account.
 - f The aperture efficiency is the fraction of the total power from an on-axis point source that is coupled to the detector. A value of 0.7 is achieved for $2FI$ horns. For the FTS short-wavelength band, the horn is significantly less than $2FI$ at the long-wavelength end of the band, resulting in a decline in the aperture efficiency²⁰.
 - g The spillover efficiency is the fraction of the detector throughput which illuminates the telescope²⁰. The remaining fraction is assumed to terminate on the cold non-emitting inside of the detector box wall, reducing the background power on the detector. A value of 0.8 is used for all photometer bands and the SSW band. For the SLW band, the spillover increases towards the long-wavelength end as the feedhorn beam gets wider.
 - h We assume an operating temperature somewhat higher than the nominal 0.3 K value to allow for significant temperature drop along the thermal straps and interfaces between the cooler evaporator and the arrays.
 - i To allow for bad channels due to possible bolometer, JFET, harness or signal chain failures in flight, we adopt a nominal 80% yield. (The measured yield of the arrays and JFETs is close to 100%.)
 - j The overall instrument transmission takes all filters, dichroics, beam dividers and mirrors into account. The value for the FTS is lower than for the photometer due to the beam divider efficiency, the larger number of optical components, and some allowance for diffraction loss in the long path length through the interferometer.

		Photometer band (mm)			FTS band (mm)	
		250	360	520	200-325	315-670
Background power/detector	PW	5.8	4.2	3.5	15	14
Background-limited NEP	W Hz ^{-1/2} x 10 ⁻¹⁷	9.8	7.0	5.3	13	16

Table 2:Background power and photon noise-limited NEPs for SPIRE.

Photometry					
λ	μm		250	360	520
ΔS (5- σ , 1-hr)	mJy	Point source (7-point mode)	3.3	3.4	3.7
		4' x 4' jiggle map	12	14	16
		4' x 8' scan map	7.9	9.2	10
Time (days) to map 1 sq. deg. to 3 mJy 1- σ			1.8	2.5	3.2
Line spectroscopy $D_S = 0.04 \text{ cm}^{-1}$					
λ	μm		200 - 315	315 - 450	450-670
ΔF (5- σ , 1-hr)	W m ⁻² x 10 ⁻¹⁷	Point source or sparse 2.6' map	7.7	6.9	6.9 - 9.6
		Fully sampled 2.6' map	23	20	20 - 29
Low-resolution spectrophotometry $D_S = 1 \text{ cm}^{-1}$					
λ	μm		200 - 315	315 - 450	450-670
ΔS (5- σ , 1-hr)	mJy	Point source or sparse 2.6' map	260	230	230 - 320
		Fully sampled 2.6' map	760	680	680-950

Table 3: Estimated sensitivity of SPIRE for photometry, line spectroscopy, and low-resolution spectrophotometry.

These sensitivity figures are only slightly different from those quoted previously in Griffin et al. (2003).²¹ A further update of the SPIRE sensitivity model is currently in progress, and will take into account as-measured instrument performance data. Preliminary results of instrument tests to date show that the instrument parameters assumed above are generally valid, although further tests and confirmation are needed for the spectrometer. However, it should be noted that, as with many cryogenic infrared space instruments, predicted sensitivity figures are subject to large uncertainties (at least a factor of two) due to uncertainties the instrument performance in flight and, in the case of SPIRE, the effective telescope background. The telescope temperature is unlikely to be much different from the assumed 80 K, but the effective emissivity is much less certain and is a critical parameter for the final sensitivity of SPIRE. The assumed value of 4% may be pessimistic: measurements on samples of the telescope mirror material²² indicate an emissivity per surface varying from 0.4% at 200 μm to 0.2% at 500 μm . But it is difficult to predict how much additional background may arise due to stray light. The design of the SPIRE bolometers has been optimised for an 80-K, 4% emissive telescope, with a background power proportional to the product of these two numbers. In the photon noise limit, the observing speed is proportional to the background power (because limiting sensitivity is proportional to the square root of the background). The SPIRE detectors can function over a wide range of background power, and are close to being photon noise limited, so they will be able to take advantage of a lower background if it obtains in orbit.

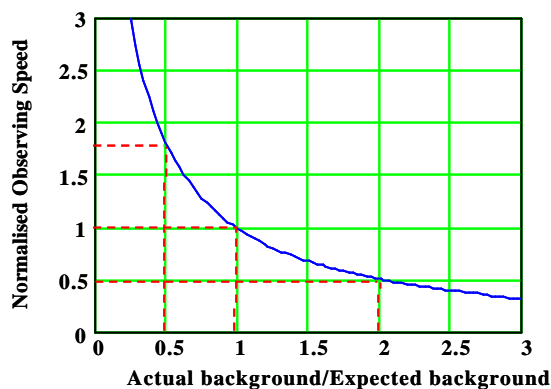


Figure 8: Normalised observing speed vs. background for the SPIRE 360- μm photometer band

Figure 8 shows the observing speed for the SPIRE 360- μm channel as a function of the overall background power, with both normalised to the design values, based on detailed modelling of the bolometer behaviour²³. In the event that the background is a factor of two higher, the observing speed is halved due to the additional photon noise; and if the background is a factor of two lower (low telescope emissivity and low stray light), then the observing speed will improve by nearly a factor of two.

Software simulators^{24,25} have been developed to model the behaviour of the photometer and FTS and produce realistic data streams that will allow instrument operating modes to be optimised and data reduction software to be evaluated.

7. CURRENT STATUS OF THE SPIRE FLIGHT INSTRUMENT PROGRAMME

A dedicated SPIRE ground testing and calibration facility²⁶ has been constructed at the Rutherford Appleton Laboratory in the UK. It has a large custom-built cryostat to house the FPU and to replicate the temperatures of the Herschel optical bench and the 1.7-K and 4.5-K stages. By means of a flip mirror, the instrument can be made to view either a large-area temperature-controlled cryogenic black body filling its beam, or it can view external sources through the cryostat window. The radiant background is set by the temperature of the cryogenic black body or by a set of cold neutral density filters when viewing outside the cryostat. A telescope simulator allows the optical characteristics of the Herschel telescope to be reproduced, and an external Fourier transform spectrometer has been installed to allow the instrument spectral response to be measured. A hot black body and a far infrared laser are available as external sources for tests requiring continuum and monochromatic input beams.

The SPIRE flight model (FM) FPU has been assembled and is currently undergoing ground testing. It contains all final flight subsystems except for the spectrometer scan mechanism, which will be installed later (a fully representative non flight unit is currently installed). Representative models of the warm electronics units are in use pending delivery of the final flight electronics. At the time of writing, two cooldown campaigns have taken place, and a third is in about to start. The FPU has also been successfully subjected to cold vibration at the Herschel cryo-vibration facility at the Centre Spatial de Liège. Instrument test results are reported in detail in several papers at this meeting^{4,10,15,16,19,27,28}. Although various problems and anomalies remain to be addressed, as is typical for the first operation of such a complex system, most performance requirements have already been demonstrated, as have many of the goals. For example, the ³He cooler performs well with the full thermal load of the five detector arrays; the bolometer noise levels as measured through the complete electronics and telemetry chain are in good agreement with the results of unit-level tests on the arrays at JPL; the overall optical efficiency of the instrument optics and filters has been estimated from measurements of the power absorbed by the bolometers and is within specification.

The Astronomical Observation Templates (AOTs) for specifying SPIRE observations have been defined and are being incorporated into Herschel scientific observation preparing tool (HSPOT) in preparation for the ESA's call for Herschel observing proposals.

8. THE SPIRE CONSORTIUM

Besides the Co-Investigators and project team members listed as the authors of this paper, many people have contributed to the technical development of SPIRE, including: Asier Abreu Araburu, Jean-Louis Augueres, Chris Brockley-Blatt, Martin Caldwell, Christophe Cara, Goutam Chattopadhyay, Riccardo Cerulli, John Coker, Patrick Collins, Dustin Crumb, Colin Cunningham, Pascal Dargent, Gary Davis, Peter Davis-Imhof, John Delderfield, Iris Didschuns, Anna Di Giorgio, Kjetil Dohlen, Lionel Duband, Roger Emery, Marc Ferlet, Didier Ferrand, Peg Frerking, Trevor Fulton, Steve Guest, Anneso Goizel, Peter Hargrave, Martin Harwit, Vic Haynes, Marty Herman, Viktor Hristov, Len Husted, Don Jennings, Brian Kiernan, Andrew Lange, Sarah Leeks, Jerry Lilienthal, Tanya Lim, John Lindner, Francoise Loubere, Bruno Maffei, Jerome Martignac, Karine Mercier, Guy Michel, Sergio Molinari, Harvey Moseley, Anthony Murphy, Jim Newell, Hien Nguyen, Seb Oliver, Renato Orfei, Ian Pain, Gary Parks, Phil Parr-Burman, Alan Pearce, Frederic Pinsard, Giampaolo Pisano, Dominique Pouliquen, Faiz Rahman, Tony Richards, Davide Rizzo, Louis Rodriguez, Samuel Ronayette, Brooks Rownd, Dominique Schmitt, Srinivasan Sethuraman, Bernhard Schulz, Bruce Sibthorpe, Sunil Sidher, Dave Smith, Locke Spencer, Brian Stobie, Rashmi Sudiwala, Kalyani Sukhatme, Jack Torrence, Carole Tucker, Anthony Turner, Tim Waskett, Mark Weilert, Berend Winter, Adam Woodcraft, Kevin Xu.

REFERENCES

1. G. Pilbratt, "Herschel Mission: status and observing opportunities", in *Space Telescopes and Instrumentation I: Optical, Infrared, and Millimeter*, Orlando, 24-31 May 2006, *Proc. SPIE* 6265 (this volume).
2. K. Dohlen, A. Orignéa, D. Pouliquen, and B. Swinyard, "Optical design of the SPIRE instrument for FIRST", *Proc. SPIE* 4013, 119, 2000.
3. P. Hargrave, J.W. Beeman, P.A. Collins, I. Didschuns, M.J. Griffin, B. Kiernan, G. Pisano, and R. Hermoso, "In-flight calibration sources for Herschel-SPIRE", *Proc. SPIE* 4850, 638, 2003.
4. P. Hargrave, T. J. Waskett, T. L. Lim, and B.M. Swinyard, "Performance of flight-model on-board calibration sources on Herschel-SPIRE", in *Millimeter and Submillimeter Detectors and Instrumentation for Astronomy III*, , Orlando, 27-31 May 2006, *Proc. SPIE* 6275.
5. I. Pain, B. Stobie, G.S. Wright, T. A. Paul, and C.R. Cunningham, "SPIRE beam steering mirror: a cryogenic two-axis mechanism for the Herschel Space Observatory". *IR Space Telescope and Instruments*, *Proc. SPIE* 4850, 619, 2003.
6. P.A.R. Ade, G. Pisano, C.E. Tucker, and S.O. Weaver, *A review of metal mesh filters*, In *Millimeter and Submillimeter Detectors and Instrumentation for Astronomy III*, , Orlando, 27-31 May 2006, *Proc. SPIE* 6275.
7. A.D. Turner, J.J. Bock, H.T. Nguyen, S. Sethuramam, J.W. Beeman, J. Glenn, P.C. Hargrave, A.L. Woodcraft, V.V. Hristov, and F. Rahman, "Si₃N₄ micromesh bolometer array for sub-millimeter astrophysics". *Applied Optics* 40, 4921, 2001.

8. B. Rownd, J.J. Bock, G. Chattopadhyay, J. Glenn, and M. Griffin, "Design and performance of feedhorn-coupled arrays coupled to submillimeter bolometers for the SPIRE instrument aboard the Herschel Space Observatory". *Proc. SPIE* 4855, 510-519, 2003.
9. G. Chattopadhyay, J.J. Bock, K. Rownd, M. Caldwell, and M. J. Griffin, "Feed horn coupled bolometer arrays for SPIRE – design, simulations and measurements", *IEEE. Trans. Microwave Theory and Techniques*, 51, 2139, 2003.
10. H.T. Nguyen. "A report of the laboratory performance of the flight bolometric detector arrays for SPIRE/Herschel", in *Millimeter and Submillimeter Detectors and Instrumentation for Astronomy III*, , Orlando, 27-31 May 2006, *Proc. SPIE* 6275.
11. B. Sibthorpe, T. J. Waskett, and M. J. Griffin, "Optimum observing modes for the Herschel/SPIRE system", in *Observatory Operations: Strategies, Processes, and Systems*, Orlando, 26-27 May 2006, *Proc. SPIE* 6270.
12. W.S. Holland, E.I. Robson, W. K. Gear, C.R. Cunningham, J.F. Lightfoot, T. Jenness, R.J. Ivison, J.A. Stevens, P.A.R. Ade, M.J. Griffin, W.D. Duncan, J.A. Murphy, and D.A. Naylor, "SCUBA: a common-user submillimetre camera operating on the James Clerk Maxwell Telescope", *Mon. Not. R. Astron. Soc.* 303, 659, 1999.
13. B.M. Swinyard, K. Dohlen, D. Ferrand, J.-P. Baluteau, D. Pouliquen, P. Dargent, G. Michel, J. Martignac, P. Ade, P. Hargrave, M. Griffin, D. Jennings, and M. Caldwell, "Imaging FTS for Herschel-SPIRE". *Proc. SPIE* 4850, 698, 1993.
14. P.A.R Ade, P.A. Hamilton, and D.A. Naylor, "An absolute dual beam emission spectrometer", *Fourier transform spectroscopy: new methods and applications*, OSA, 90, 1999.
15. L.D. Spencer, D.A. Naylor, and B.M Swinyard. "A comparison of the theoretical and measured performance of the Herschel/SPIRE imaging Fourier Transform Spectrometer", in *Space Telescopes and Instrumentation I: Optical, Infrared, and Millimeter*, Orlando, 24-31 May 2006, *Proc. SPIE* 6265 (this volume).
16. D.A. Naylor, J-P. Baluteau, P. Davis-Imhof, M.J. Ferlet, T.R. Fulton, and B.M. Swinyard., "Performance evaluation of the Herschel/SPIRE imaging Fourier Transform Spectrometer", in *Space Telescopes and Instrumentation I: Optical, Infrared, and Millimeter*, Orlando, 24-31 May 2006, *Proc. SPIE* 6265 (this volume).
17. J.V. Lindner, D.A. Naylor, and B.M. Swinyard. "SHIFTS: a simulator for the Herschel imaging Fourier transform spectrometer", in *Space Telescopes and Instrumentation I: Optical, Infrared, and Millimeter*, Orlando, 24-31 May 2006, *Proc. SPIE* 6265 (this volume).
18. L. Duband, "Spaceborne helium adsorption coolers", Proceedings of ESA Symposium on *The Far Infrared and Submillimetre Universe*, Grenoble, 15-17 April 1997, *ESA SP-401*, 357, 1997.
19. P. Hargrave, J.J. Bock, C. Brockley-Blatt, J. Coker, L. Duband, A. Goizel, D.K. Griffin, and B.M. Swinyard, "The 300 mK system for Herschel-SPIRE", in *Millimeter and Submillimeter Detectors and Instrumentation for Astronomy III*, , Orlando, 27-31 May 2006, *Proc. SPIE* 6275.
20. M.J. Griffin, J.J. Bock, and W.K. Gear, "Relative Performance of Filled and Feedhorn-Coupled Focal Plane Architectures", *Applied Optics*, 31, 6543, 2003.
21. M.J. Griffin, B.M. Swinyard, and L. Vigroux. "SPIRE - Herschel's submillimeter camera and spectrometer", *Proc. SPIE* 4850, 686, 2003.
22. J. Fischer, T. Klassen, N. Hovenier, G. Jakob, A. Poglitsch, and O. Sternberg "Cryogenic far-infrared laser absorptivity measurements of the Herschel Space Observatory telescope mirror coatings", *Applied Optics*, 43, 3765, 2004.
23. R.V. Sudiwala, M.J. Griffin, and A.L. Woodcraft, "Thermal modelling and characterisation of semiconductor bolometers", *Int. Journal of Infrared and Mm Waves*, 23, 545, 2002.
24. B. Sibthorpe, A.L. Woodcraft, and M.J. Griffin, "A software simulator for the Herschel-SPIRE imaging photometer", *Proc. SPIE* 5487, 2004.
25. J. Lindner, D. Naylor, and B. Swinyard, *Simulation of the performance of ESA's Herschel/SPIRE imaging Fourier transform spectrometer*, *Proc. SPIE* 5487, Glasgow, 21-25 June 2004.
26. P.A. Collins, D.L. Smith, M. Ferlet, T. Grundy, M. Harman, M.J. Griffin, P.A.R. Ade, and B.M. Swinyard, *Ground calibration facility for Herschel-SPIRE*. *Proc. SPIE* 4850, 628-637, 2003.
27. B.M. Swinyard, K. Dohlen, M. Ferlet, J. Glenn, and J. Bock, "Optical performance and characterisation of Herschel/SPIRE", in *Space Telescopes and Instrumentation I: Optical, Infrared, and Millimeter*, Orlando, 24-31 May 2006, *Proc. SPIE* 6265 (this volume).
28. T.L. Lim, B.M. Swinyard, A. Abreu Aramburu, J.J. Bock, M.J. Ferlet, T.R. Fulton, D.K. Griffin, M.J. Griffin, S.J. Leeks, D.A. Naylor, D. Rizzo, E.C. Sawyer, B. Schulz, S.D. Sidher, L.D. Spencer, D.L. Smith, T.J. Waskett, and A.L. Woodcraft, "Preliminary results from Herschel-SPIRE flight model testing", in *Space Telescopes and Instrumentation I: Optical, Infrared, and Millimeter*, Orlando, 24-31 May 2006, *Proc. SPIE* 6265 (this volume).